SUPPLEMENTARY INFORMATION

Effect of channel patterning precision on the performances of vertical OECTs

Ruhua Wu [a], Chufeng Wu [a], Jinhao Zhou [a], Liang-Wen Feng [b], Jianhua Chen [c], Dan Zhao *[a], and Wei Huang *[a]

a. School of Automation Engineering, University of Electronic Science and Technology of China (UESTC), 611731, Chengdu, China.
b. Key Laboratory of Green Chemistry & Technology, Ministry of Education, College of Chemistry, Sichuan University, Chengdu,610065, China.
c. Department of Chemical Science and Technology, Yunnan University, Kunming, China.

Supplementary Figures:

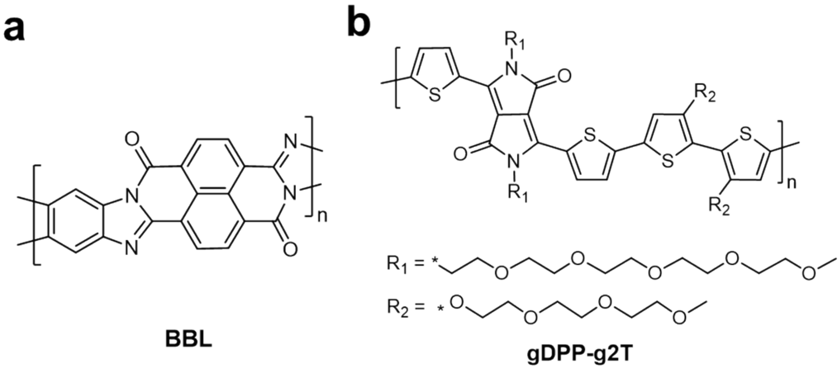

Figure S1. Chemical structures of BBL (a) and gDPP-g2T (b).

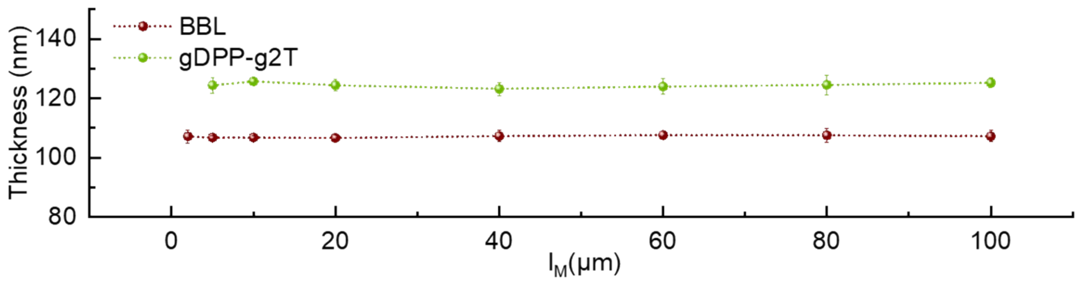

Figure S2. Plot of thickness of BBL and gDPP-g2T thin films with different patterning precisions (Error bars represent the standard deviation of 3 data points). The BBL and gDPP-g2T films hold average thicknesses of approximately 107 nm and 124 nm, respectively, under various l_M. Therefore, patterning precision would not affect the thickness of the OMIECs, and it also indicates that the device performance variation is due to different l_M.

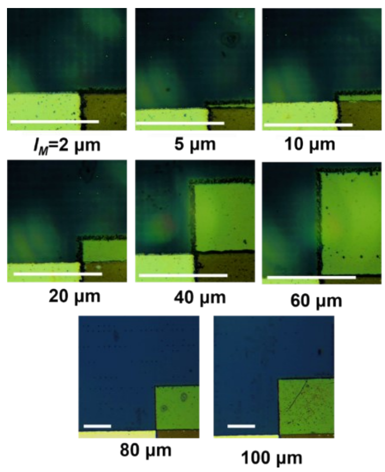

Figure S3. Microscopic images of the BBL thin films with different patterning precisions. (scale bar =50 μm)

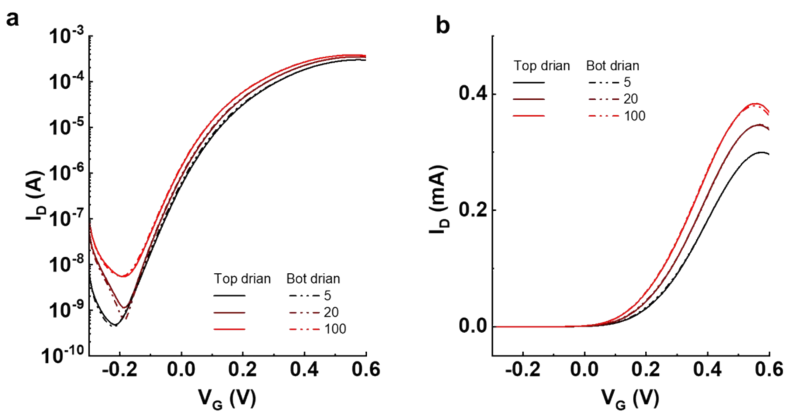

Figure S4. Transfer characteristics in log-scale (a) and linear scale (b) of BBL-based vOECTs, where the block and dash curves represent the drain terminal set at the top and bottom electrode, respectively.

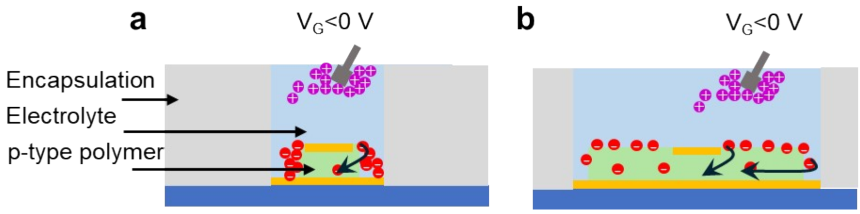

Figure S5. Schematics of comparing ion injection of precise pattern (a) and large pattern (b) of a p-type accumulation-mode vOECT.

Taking a p-type accumulation-mode vOECT as an example, when the negative gate bias gradually increases, the stronger accumulation of ions at the semiconductor-electrolyte interface of precisely patterned vOECT may result in stronger Coulombic repulsion, affecting ion doping efficiency. Moreover, larger OMIEC introduces a larger contact area between the electrodes and channel, leading to smaller inject resistance, which could also facilitate the injection of ions and negatively shifted V_{th} for n-type transistors or positively shifted V_{th} for p-type transistors.

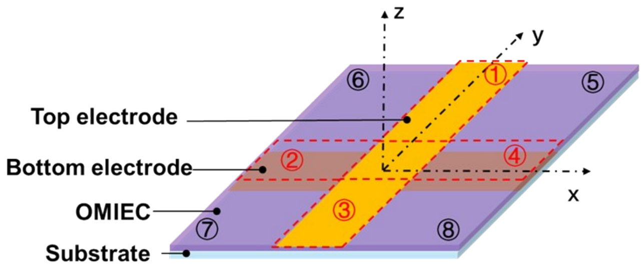

Figure S6. Schematic of a vOECT with redundant channel area and its spatial coordinate system. Note that the model only considers the parts where OMIEC films directly contacting electrodes (area 1-4), excluding the parts of 5-8.

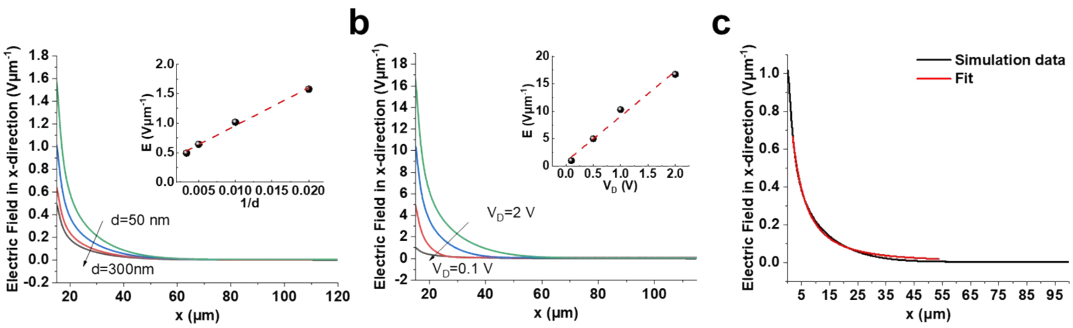

Figure S7. Simulation curves of the fringe electric field as a function of OMIEC thickness *d* (a), source-drain voltage V_D (b), and the fitting curve with $E_{fr} \propto x^{-2}$.

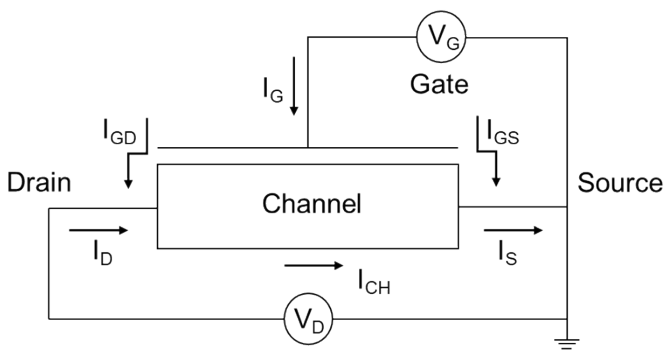

Figure S8. Circuit diagram describing the current discrete model of OECT.

It shows a circuit diagram of the discrete model with the gate current branches I_S, I_D, and I_{CH}[1]. Based on this model, a dynamic model describing the source/drain current is proposed.

$$i_D(t) = i_{CH}(t) - f i_G(t) \tag{1}$$

$$i_S(t) = -i_{CH}(t) - (1 - f) i_G(t) \tag{2}$$

f is a weighting factor, supposed to be related to the bias at drain/gate terminals and device symmetry[2, 3]. At the off-state of vOECTs, pristine BBL exhibits the property of an intrinsic semiconductor with a conductivity under 10^{-12} S cm^{-1}.[4] In this case, I_{CH} contributes little to I_D but dominated by $I_{G.}$ It suggests that the drain current at off-state (I_{off}) exhibits a similar trend to I_G as l_M increases regarding increasing parasitic impedance.

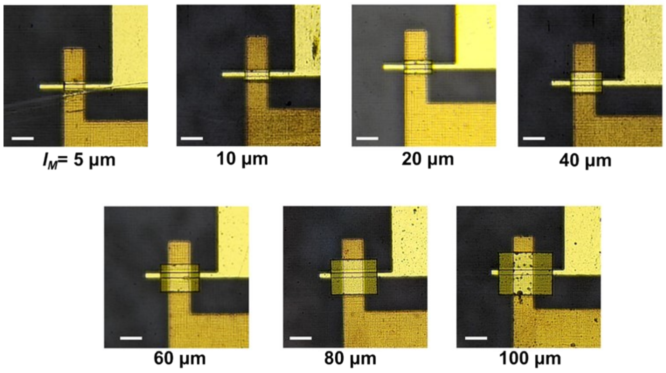

Figure S9. Microscopic images of the BBL-based vOECTs with 100 μm wide top electrodes (scale bar =100 μm).

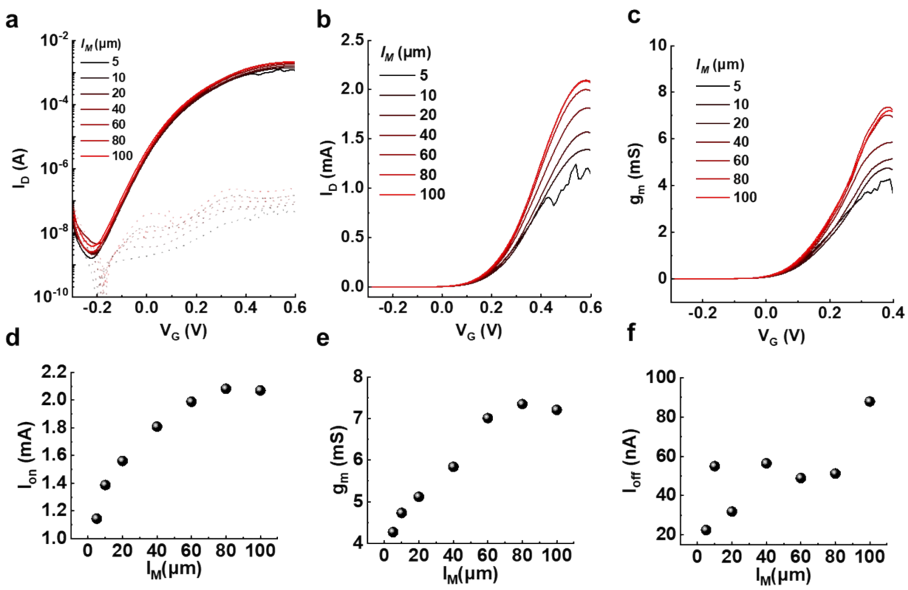

Figure S10. Transfer characteristics (V_D = 0.1 V) in log-scale (a) and linear scale (b), and plots of g_m (c) of BBL-based vOECTs with top electrode width of 100 μm. I_{on} (d),

g_m (e), and I_{off} (f) of the BBL-based vOECTs.

BBL-based vOECTs with wider top electrodes (W_T = 100 μm) are prepared (Figure S9). Transfer characteristics are performed along with the extraction of several key parameters, as shown in Figure S10. Compared to the vOECT with a top electrode width of approximately 30 μm, the vOECT with a top electrode width of 100 μm exhibits about a threefold increase in I_{on} and g_m. As l_M increases from 5 μm to 100 μm, I_{on} and g_m of the vOECT increase from 1.14 mA and 4.27 mS to 2.01 mA and 7.21 mS, respectively. The parameters gradually reach a plateau as l_M increases to 60 μm, exhibiting a similar trend to the devices with the narrower top electrode. However, due to the larger area of top electrodes, the electrolyte-gold electrode contact area is significantly large. I_{off} is adversely affected due to additional parasitic impedance, resulting in high I_{off} at 10^{-8}-10^{-7} A, which is an order of magnitude larger than the narrower top OECTs.

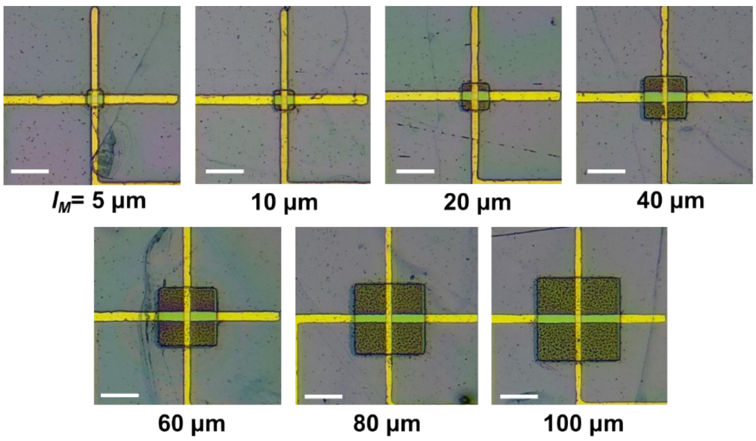

Figure S11. Microscopic images of the gDPP-g2T-based vOECTs with different patterning precisions (scale bar =100 μm).

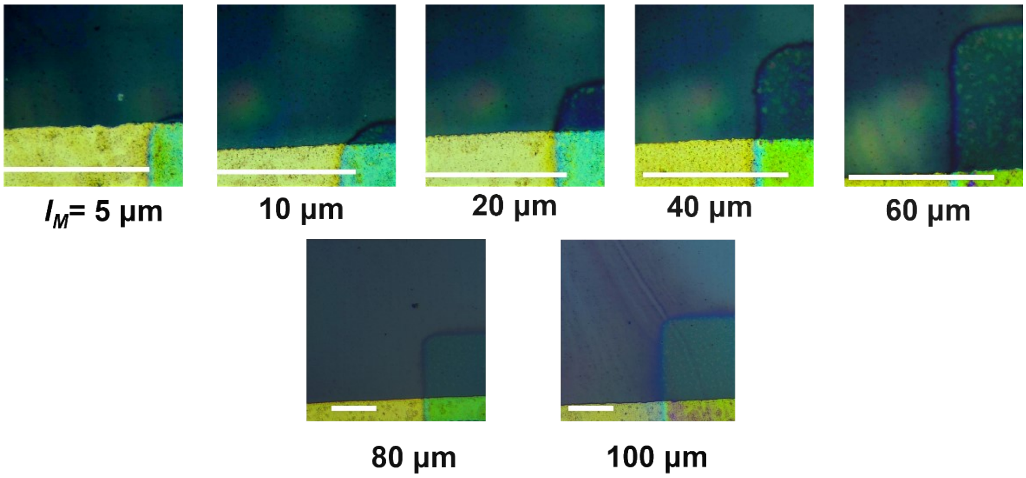

Figure S12. Microscopic images of the gDPP-g2T thin films with different patterning precisions. (scale bar =50 µm)

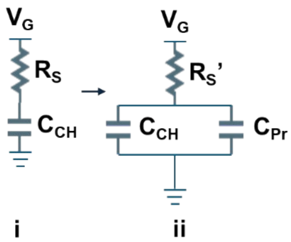

Figure S13. Ionic equivalent circuit of an ideal OECT (i) and an OECT with considering its parasitic impedance (ii).

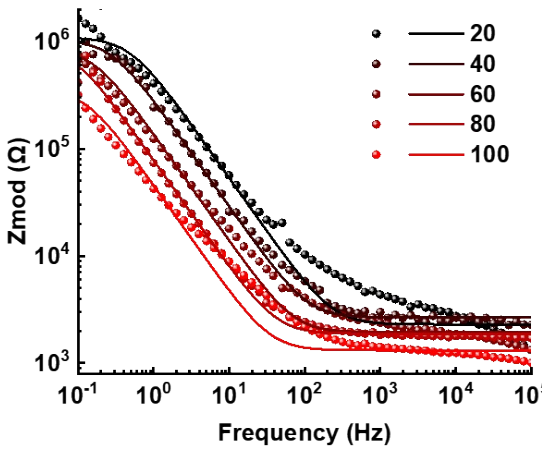

Figure S14. EIS curves of the n-type vOECTs with different l_M (See Experimental for detailed measurement setup).

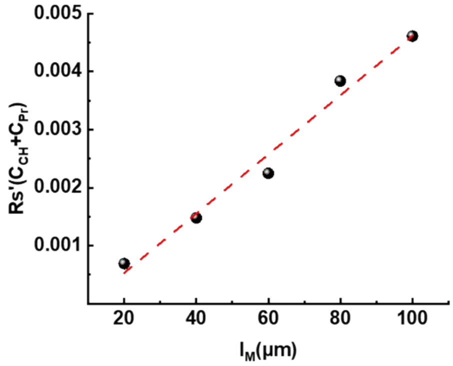

Figure S15. Plot of $R_S^{'}(C_{CH} + C_{Pr})$ as a function of l_M and the corresponding linear fitting line.

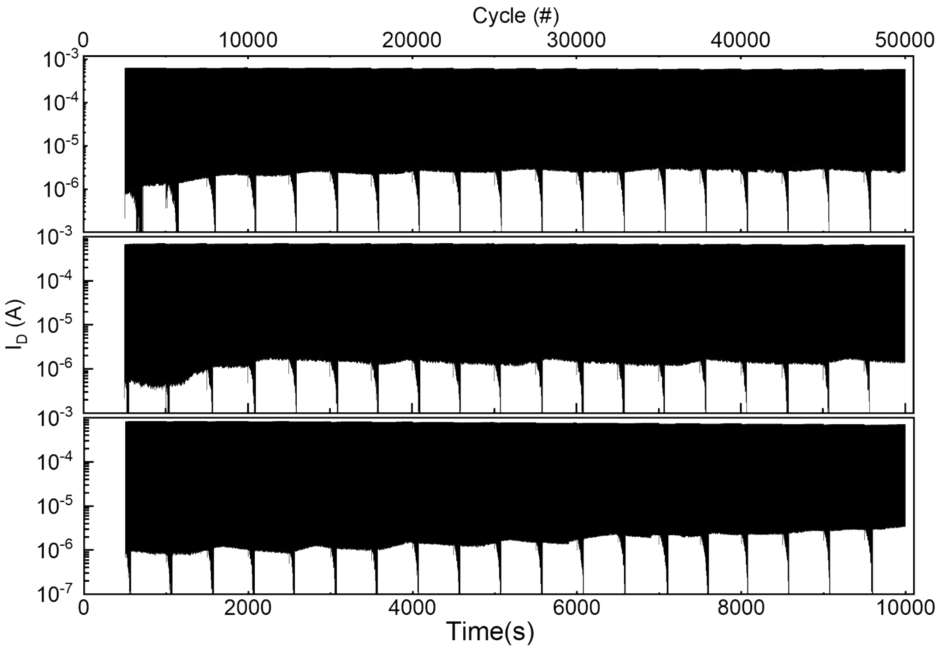

Figure S16. Cycling stability characteristics (after initializing cycles) of BBL-vOECTs with l_M of 5, 40, and 100 μm.

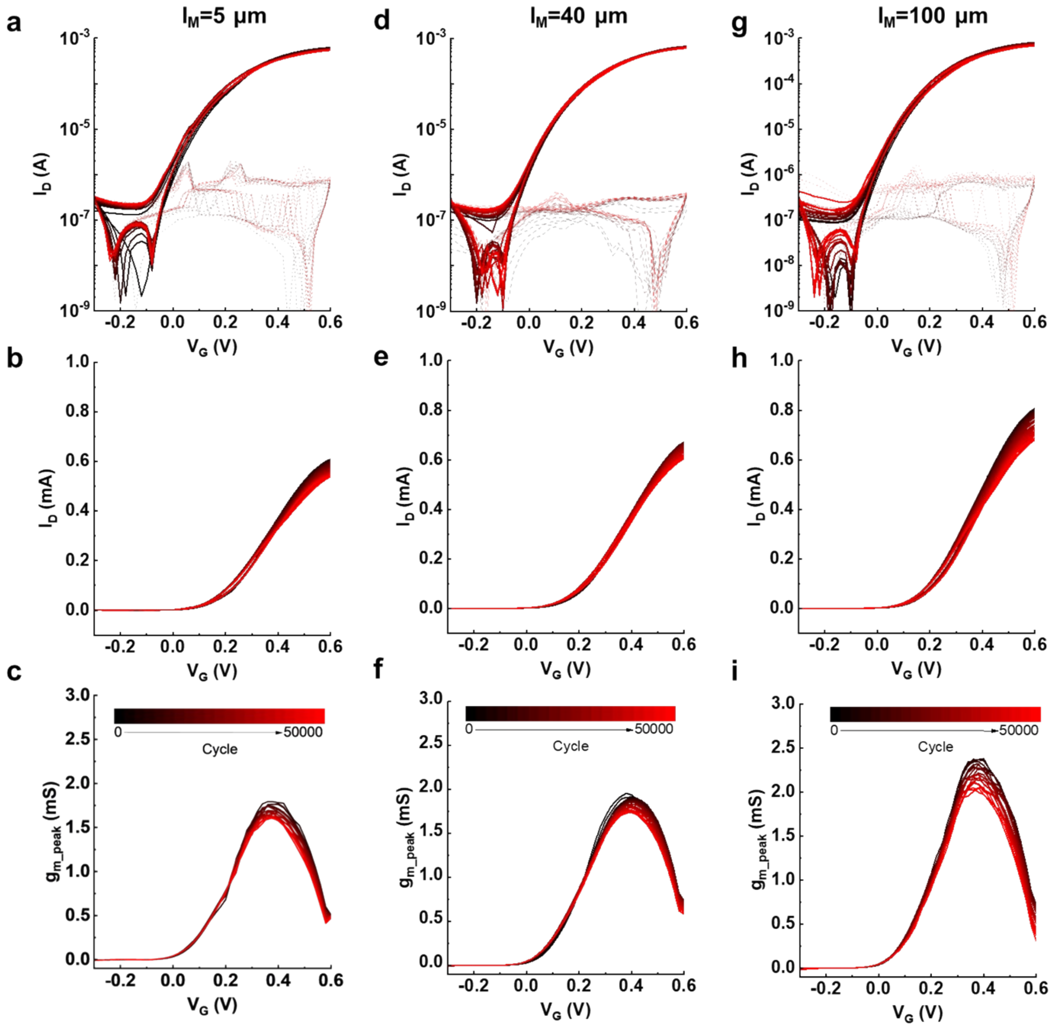

Figure S17. Transfer characteristics in log (a,d,g) and linear scale (b,e,h) and transconductance plot (c,f,i) of BBL-vOECTs with l_M = 5 μm (a-c), 40 μm (d-f) and 100 μm (g-i), respectively, during the cycling stability characteristics.

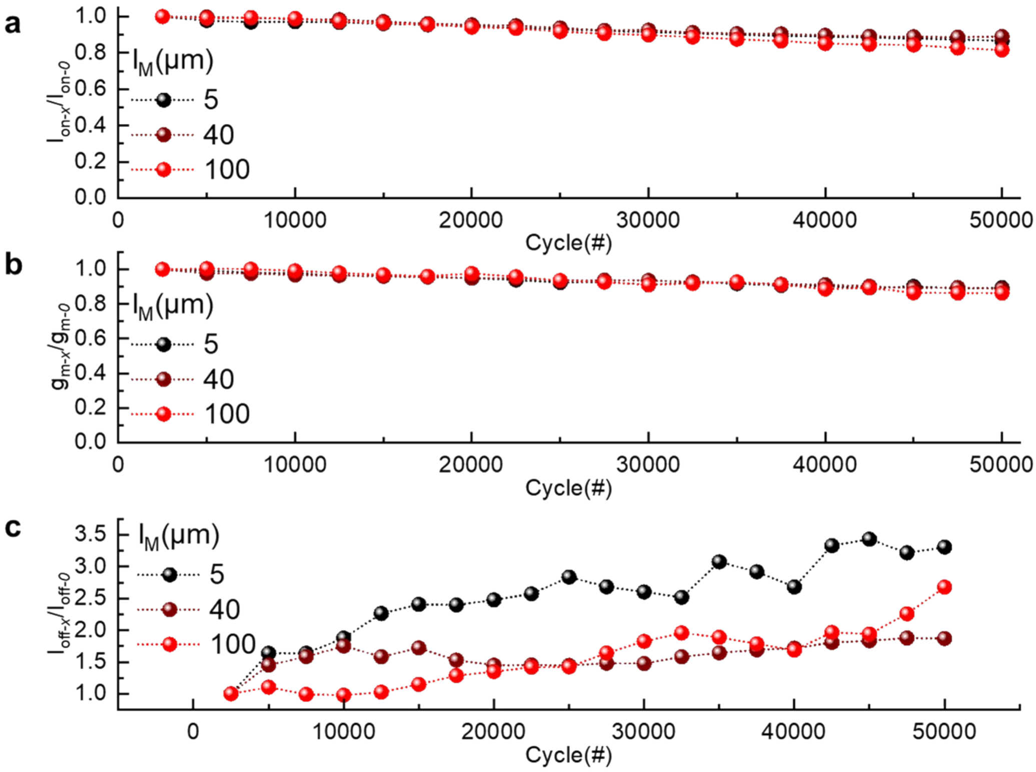

Figure S18. Decay trends of (a) I_{on}, (b) g_{m_peak} and (c) I_{off} during cycling characterizations.

Supplementary Tables

Table S1. The thickness of BBL and gDPP-g2T thin films

		l_M (μm)							
		2	**5**	**10**	**20**	**40**	**60**	**80**	**100**
Thickness (nm)	**gDPP-g2T**	/	124.41 ±2.63	125.73 ±1.06	124.42 ±2.02	123.21 ±2.20	123.98 ±2.68	124.53 ±3.25	125.24 ±1.56
	BBL	107.17±2.20	106.80 ±0.52	106.79 ±0.50	106.68 ±1.10	107.32 ±1.89	107.63 ±1.28	107.58 ±2.32	107.26 ±1.92

Table S2. Parameters for simulations

	Parameters	**Values**	**Reference**
Configuration	Electrode Overlap	30 μm	-
BBL	Permittivity	8.3	5
	Band gap	1.8 eV	6
	Work function	4.3 eV	6
	Electron mobility	2.2×10^{-2}cm^2/V	6
	Bandgap narrowing	None	-
Environment	Temperature	300 K	-
	Ambient	Air	-

The distribution of the fringe electric field was obtained by using Lumerical Charge simulations. Table S1 shows the device configuration, environment, and BBL material parameters, along with relevant references.

References

1. Friedlein, J. T.; Donahue, M. J.; Shaheen, S. E.; Malliaras, G. G.; McLeod, R. R., Microsecond Response in Organic Electrochemical Transistors: Exceeding the Ionic Speed Limit. *Advanced Materials* **2016,** *28* (38), 8398-8404.
2. Faria, G. C.; Duong, D. T.; Salleo, A., On the transient response of organic electrochemical transistors. *Organic Electronics* **2017,** *45*, 215-221.
3. Friedlein, J. T.; McLeod, R. R.; Rivnay, J., Device physics of organic electrochemical transistors. *Organic Electronics* **2018,** *63*, 398-414.
4. Fazzi, D.; Negri, F., Addressing the Elusive Polaronic Nature of Multiple Redox States in a π-Conjugated Ladder-Type Polymer. *Advanced Electronic Materials* **2021,** *7* (1), 2000786.
5. Kraner, S.; Koerner, C.; Leo, K.; Bittrich, E.; Eichhorn, K. J.; Karpov, Y.; Kiriy, A.; Stamm, M.; Hinrichs, K.; Al-Hussein, M., Dielectric function of a poly(benzimidazobenzophenanthroline) ladder polymer. *Physical Review B* **2015,** *91* (19), 195202.
6. Kim, F. S.; Park, C. H.; Na, Y.; Jenekhe, S. A., Effects of ladder structure on the electronic properties and field-effect transistor performance of Poly(benzobisimidazobenzophenanthroline). *Organic Electronics* **2019,** *69*, 301-307.